# Error Compensation of the Temperature Influence on Radar Based Displacement Measurements

Christoph Will[1], Sebastian Mann[1], Fabian Michler[1], Torsten Reissland[1], Fabian Lurz[1], Robert Weigel[1], and Alexander Koelpin[2]

[1]Institute for Electronics Engineering, Friedrich-Alexander University of Erlangen-Nuremberg, 91058 Erlangen, Germany
Phone: +49(0)9131 85-27190, Email: christoph.will@fau.de

[2]Chair for Electronics and Sensor Systems, Brandenburg University of Technology, 03046 Cottbus, Germany

***Abstract*—Highly precise sensor systems for contactless displacement measurements play an important role within the industrial application field. Various radar based measurement systems utilizing different techniques have been published for this purpose, but the influence of the ambient temperature on the measurement results has only rarely been investigated, yet. Whereas many publications deal with research on temperature compensation of single components, this paper examines the influence of the ambient temperature on the entire RF front end of the sensor system, a 61 GHz Six-Port microwave interferometer. After presenting the measurement system, the temperature influences on the four output voltages and the consequences for the measurement results are analyzed. In the main part of this paper a compensation algorithm is proposed to significantly decrease the temperature induced impairments of the systematic measurement error.**

***Index Terms*—Calibration, electromagnetic measurements, error compensation, radar interferometry, radar signal processing, temperature dependence.**

## I. Introduction

Many industrial applications require precise distance, thickness, displacement or vibration measurements. Radar based sensor systems represent an emerging method for this purpose since they address a large application spectrum by reason of their robustness, low costs, and contactless measurement technique. Depending on the specific application scenario the appropriate radar technique can be utilized, like Doppler, frequency-modulated continuous-wave, continuous-wave (CW) or ultra-wideband. For applications that require only relative displacement measurements the CW radar technique is beneficial. One low-cost as well as low-power implementation of CW radar is the Six-Port microwave interferometer featuring high phase accuracy. Introduced in the 1970s for power measurements purpose [1], the Six-Port principle has been increasingly used for radar interferometry in the latest years. Meanwhile, a variety of calibration and error correction algorithms as well as several application options have been published for Six-Port microwave interferometers [2].

Especially in the industrial application field a system calibration along the relevant measurement range is mandatory. Whereas hardware based approaches with known calibration standards, like open/short/match [3], imply a huge calibration effort, software based error correction methods utilizing independent measurements at known target positions are preferred [4]. The published calibration algorithms assume a constant ambient and front end (FE) temperature, but do not deal with the influences of temperature changes on the measurement results. Other publications propose temperature stabilized or compensated circuits for electronic components like diode detectors [5], low noise amplifiers (LNA) [6], and voltage controlled oscillators (VCO) [7]. In this paper the temperature influence on the entire RF part of the measurement system is discussed, its consequences on the measured quantity values are analyzed and a temperature compensating algorithm to decrease the systematic measurement error is proposed.

## II. Measurement System

The used sensor system for the displacement measurements is a monostatic Six-Port microwave interferometer whose block diagram is depicted in Fig. 1. A phase-locked loop stabilized VCO, operating in the 61 GHz industrial, scientific, and medical (ISM) band, generates an electromagnetic signal that is equally split by a 3 dB radar coupler. One portion is emitted by a near-field antenna, the other portion is fed via a variable diode based attenuator to the reference input of the Six-Port network. The other Six-Port input port is fed by the reflected signal which is beforehand amplified by an LNA.

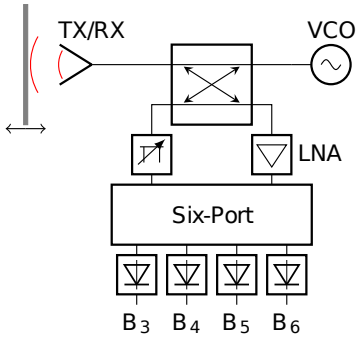


Fig. 1. Block diagram of the Six-Port sensor.

The two input signals are superimposed within the Six-Port network with relative phase shifts of multiples of $\pi/2$ between them which leads to two differential output signal pairs that are orthogonal to each other. The four resulting output signals are down-converted by Schottky diode detectors to the baseband voltages $B_{3...6}$. Four synchronized analog-to-digital converters (ADC) each with a resolution of 24 bit are

used to simultaneously sample these baseband voltages. Due to their orthogonality, the two differential output signal pairs can be interpreted as in-phase and quadrature (I/Q) components of a complex signal representation. As the argument of a complex value represents its phase information, the four baseband voltages can be utilized to calculate the relative phase shift $\Delta\sigma$ between both input signals:

$$\Delta\sigma = \arg\{(B_5 - B_6) + j(B_3 - B_4)\}. \quad (1)$$

Since a moving target produces a phase shift of the reflected signal, relative target displacements $\Delta d$ can be calculated using the known wavelength $\lambda$:

$$\Delta d = \Delta\sigma \cdot \frac{\lambda}{4\pi}. \quad (2)$$

A metallic plate is used as target which is mounted on a high precision linear stage. The target position can be swept by $\pm 2.0$ mm from the origin situated in 2.0 cm distance from the antenna. The Six-Port sensor as well as the linear stage with the target are placed within a temperature chamber, but the printed circuit board with the ADC remains outside. The linear stage, the temperature chamber, and the ADC board are controlled by a personal computer which is additionally used for further signal processing by MATLAB.

## III. Temperature Influence

As described in the previous sections, several components of the Six-Port sensor have temperature dependent output characteristics. Nowadays, there exist temperature stabilized circuits for VCO/PLL [7] and LNA [6], but nevertheless, these component types still have a remaining temperature dependency. Other and more important components are the Schottky diode based detectors, which have a known high temperature dependency [5], [8], and the diode based variable attenuator in the reference path. In [9] the temperature dependent diode current is described as

$$I_D(T) = I_S(T) \cdot \left[ e^{\left(\frac{V_D}{n \cdot V_T(T)}\right)} - 1 \right] \quad (3)$$

whereas the reverse bias saturation current is

$$I_S(T) = I_S(T_0) \cdot e^{\left(\frac{T}{T_0} - 1\right) \cdot \frac{V_G(T)}{n \cdot V_T(T)}} \cdot \left(\frac{T}{T_0}\right)^{\frac{\chi}{n}} \quad (4)$$

and the thermal voltage can be expressed as

$$V_T(T) = \frac{k \cdot T}{q}. \quad (5)$$

Within these formulas, $V_D$ describes the voltage across the diode, $V_G(T)$ is the gap voltage, $n$ is the ideality factor, $\chi$ is the temperature coefficient, and $T_0$ equals 300 K. Since an analytical calculation of the temperature dependent diode characteristic is difficult due to the dependency between $V_D$ and $I_D$, the voltage/temperature-characteristics for the detectors was simulated using *Keysight ADS* by utilizing the exported design data from *CST Microwave Studio*. The simulation results for a temperature span of 30...80 °C and an input power of -15 dBm are depicted in Fig. 2.

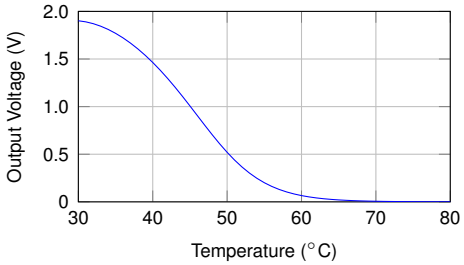


Fig. 2. Simulated detector output voltage over the diode temperature for an input power $P_{in}$ of -15 dBm.

During measurements the target was moved once along the complete measurement range (-2.0...2.0 mm) with a step size of 20 µm for each temperature. The temperature span was defined as 15...30 °C with a step size of 1.0 °C. Five iterations per temperature setting were done since the chamber regulates the setting within a range of $\pm 1.0$ °C. At each measurement point 1000 samples per baseband voltage were acquired and averaged, and the front-end (FE) temperature was measured by accessing an integrated sensor within the VCO. The influence of the FE temperature on one exemplary baseband voltage ($B_5$) along the complete measurement range is plotted in Fig. 3, whereas the single measurement iterations are sorted by the mean FE temperature along the measurement range.

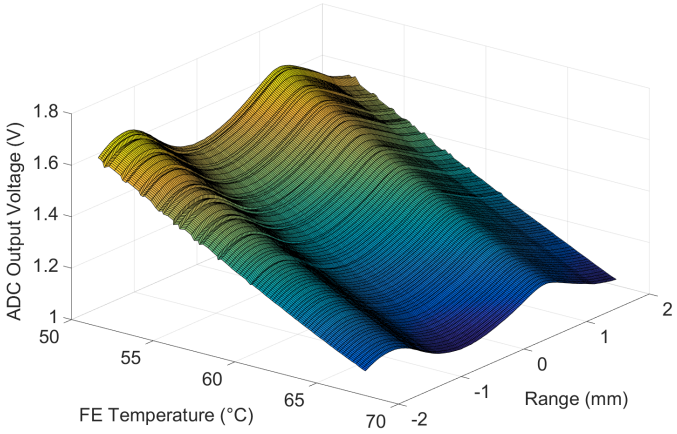


Fig. 3. Influence of the temperature on the detector output voltage for baseband signal $B_5$.

All baseband voltages show a rather linear dependency from the FE temperature within the measured range of approximately 52...68 °C, which does not fit to the simulation results in Fig. 2. One explanation is the temperature gradient over the FE which leads to lower temperatures at the detectors than at the VCO being the main heat source. Another reason is the superposition of the various temperature dependency effects of the different FE components.

## IV. Temperature Compensation

Since all sampled baseband voltages $V_{ADC,i}$ with $i = 3...6$ show a rather linear dependency from the measured FE temperatures $T_{FE,i,j}$ within their measured ranges, an individual

linear fit is performed per baseband signal $i$ at each target distance $j$:

$$V_{ADC,i,j} = a_{i,j} \cdot T_{FE,i,j} + b_{i,j}. \quad (6)$$

The gradients $a_{i,j}$ of the fitted lines vary with a standard deviation less than $1.2 \cdot 10^{-3}$ only slightly along the measurement range for each measured baseband voltage $V_{meas,i}$, for which reason their mean values $a_i$ are used to compensate each baseband value as follows:

$$V_{comp,i} = V_{meas,i} + a_i \cdot (T_{FE,0} - T_{FE,i}), \quad (7)$$

in which $T_{FE,0}$ is an arbitrarily chosen reference FE temperature. Here, $T_{FE,0}$ is defined as 60.0 °C which equals approximately the mean value of the investigated temperature span during measurements. The dependency of one exemplary baseband signal ($B_5$) for a stationary target plotted over both the temperature within the chamber $T_C$ and the FE temperature $T_{FE}$, as well as their fitted lines are depicted in Fig. 4.

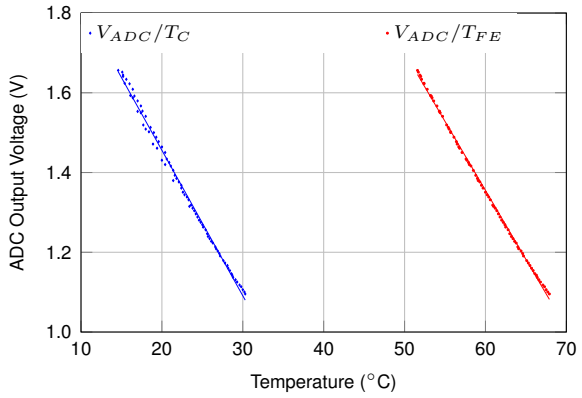


Fig. 4. Temperature dependent voltage changes of a single baseband signal for a stationary target plotted together with their linear fitting curves.

After this temperature compensation based calibration of the measurement scenario, the measured baseband voltages are individually compensated for each location within the measurement range by utilizing (7). The area $VA_{raw}$ of the raw exemplary baseband voltage $B_5$ along the swept distance for the complete calibrated temperature span as well as the resulting voltage area $VA_{comp}$ after compensation are illustrated in Fig. 5. The voltage ranges of this exemplary baseband signal are depicted in Fig. 6, prior to ($VR_{raw}$) as well as after ($VR_{comp}$) temperature compensation. Here, the term *voltage range* states the range between maximal and minimal voltage value of a baseband signal at a specific target position due to a varying ambient temperature span of 15...30 °C. Both figures clearly show an improved stability regarding a varying ambient temperate of the exemplary baseband signal if applying the proposed compensation technique. The mean values over the measurement range as well as the standard deviations of both raw and compensated voltage ranges of all baseband signals are compared among each other in Tab. I. One resulting conclusion is that the temperature influence on the voltage ranges of the baseband signals increases the higher the mean

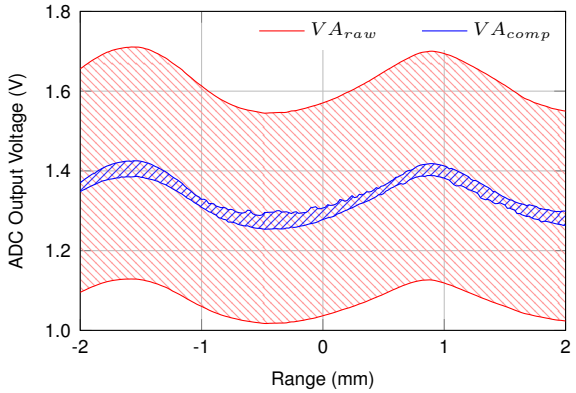


Fig. 5. Voltage areas of a raw baseband signal and its compensation result along the swept distance for a varying ambient temperature span of 15...30 °C.

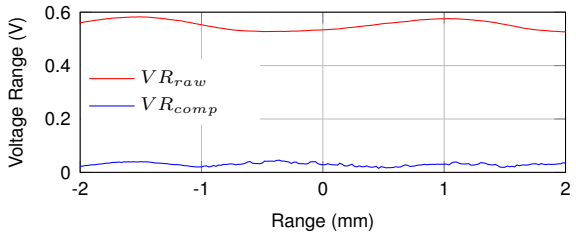


Fig. 6. Voltage ranges of a raw baseband signal and its compensation result due to a varying ambient temperature span of 15...30 °C.

values of the single raw baseband voltages $V_{raw,mean}$ are. The significant decrease of the mean values of the voltage ranges as well as their standard deviations by temperature compensation, independent of the arithmetic averages of the baseband voltages, represents an additional conclusion.

Considering (1), the four baseband voltages are interpreted as differential I/Q components for a subsequent phase evaluation in further signal processing. Since regarding (2) relative target displacements are linear dependent of the calculated phase, the resulting effects of the temperature influence and its compensation on the complex signal representation have to be examined as well. Nonidealities in the RF part of the Six-Port sensor deform the unit circle as the ideal complex representation to an offset ellipse which results in a highly nonlinear phase curve. Therefore, to minimize the phase nonlinearity during measurements, an ellipse fitting for I/Q imbalance compensation [10] is applied for the measured quantity values at the reference temperature $T_{FE,0} = 60.0$°C. This reference

TABLE I
COMPARISON OF THE MEAN VOLTAGE RANGES AND THEIR STANDARD DEVIATIONS OF RAW AND COMPENSATED BASEBAND SIGNALS.

| Baseband signal | 3 | 4 | 5 | 6 |
|---|---|---|---|---|
| $V_{raw,mean}$ (mV) | 793.1 | 1190.2 | 1338.6 | 940.5 |
| $VR_{raw,mean}$ (mV) | 323.8 | 500.8 | 553.5 | 396.8 |
| $VR_{raw,std}$ (mV) | 8.0 | 16.1 | 18.7 | 11.5 |
| $VR_{comp,mean}$ (mV) | 15.3 | 31.0 | 30.2 | 20.6 |
| $VR_{comp,std}$ (mV) | 3.2 | 5.8 | 6.5 | 4.4 |

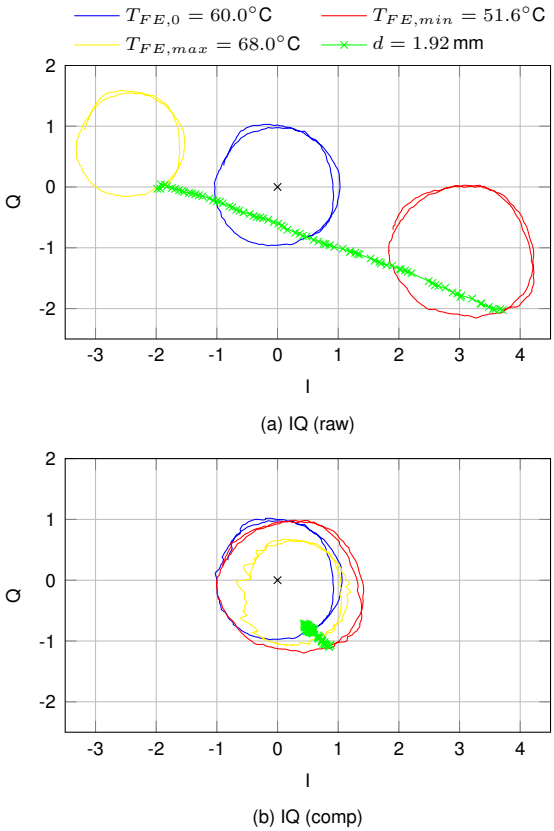


Fig. 7. Temperature influence on the complex representation of the measured baseband signals.

ellipse is utilized for I/Q imbalance compensation within all other measurements. The resulting ellipse compensated complex representations for various FE temperatures are shown in Fig. 7. In sub-plot (a), in which no temperature compensation is applied, the complex representations are significantly shifted within the complex plane due to the FE temperature deviations. For temperature deviations larger than approximately 2.5°C from the reference temperature the reconstructed complex representations do not cover the total circle around the complex origin anymore which implies an incorrect phase evaluation. Sub-plot 7(b) shows that these temperature induced shifts are minimized by temperature compensation and an incorrect phase evaluation is prevented.

The maximal systematic measurement error along the measurement range of -2.0 mm. . . 2.0 mm is plotted over the mean FE temperature in Fig. 8 for using both the raw and compensated baseband voltages. Here, temperature compensation implicates better results in the complete investigated temperature span. The temperature induced shifts of the complex representation for uncompensated measurements explains the significant increase of the corresponding error curve.

## V. Conclusion

In this paper the investigation of the temperature influence on a radar based displacement measurement system was presented, along with a compensation method to significantly decrease the temperature induced impairments of the systematic measurement error. For deriving the compensation strategy the temperature dependency of the sensor system as a whole had to be examined in the relevant temperature span. The presented compensation by individual, temperature dependent, linear shifts of the single measured quantity values is referred to their behavior at an arbitrarily chosen reference temperature. The residual temperature induced error on the measured distance has been reduced from several millimeters to below half a millimeter for a temperature span of approximately 15 °C.

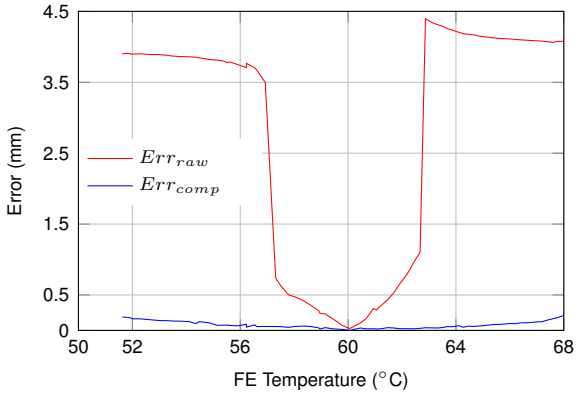


Fig. 8. Comparison of the maximal systematic measurement error along the measurement range between raw and compensated measurement results for different FE temperatures using 60 °C as a reference.

## References


[1] G. F. Engen and C. A. Hoer, "Application of an arbitrary 6-port junction to power-measurement problems," *Instrumentation and Measurement, IEEE Transactions on*, vol. 21, no. 4, pp. 470–474, Nov 1972.

[2] A. Koelpin, F. Lurz, S. Linz, S. Mann, C. Will, and S. Lindner, "Six-Port based interferometry for precise radar and sensing applications," *Sensors*, vol. 16, no. 10, p. 1556, 2016. [Online]. Available: http://www.mdpi.com/1424-8220/16/10/1556

[3] S. Li and R. G. Bosisio, "Calibration of multiport reflectometers by means of four open/short circuits," *IEEE Transactions on Microwave Theory and Techniques*, vol. 30, no. 7, pp. 1085–1090, Jul 1982.

[4] K. Staszek, S. Linz, F. Lurz, S. Mann, R. Weigel, and A. Koelpin, "Improved calibration procedure for Six-Port based precise displacement measurements," in *2016 IEEE Topical Conference on Wireless Sensors and Sensor Networks (WiSNet)*, Jan 2016, pp. 60–63.

[5] M. Hoefle, A. Penirschke, A. Amrhein, O. Cojocari, M. Trier, and R. Jakoby, "Addressing the temperature stability in an 89 GHz Schottky detector design for radiometry," in *2012 37th International Conference on Infrared, Millimeter, and Terahertz Waves*, Sept 2012, pp. 1–3.

[6] S. Kawai, T. Wang, T. Mitomo, and S. Saigusa, "A temperature variation tolerant 60 GHz low noise amplifier with current compensated bias circuit," in *2013 IEEE Asian Solid-State Circuits Conference (A-SSCC)*, Nov 2013, pp. 429–432.

[7] V. Ravinuthula and S. Finocchiaro, "A low power high performance PLL with temperature compensated VCO in 65nm CMOS," in *2016 IEEE Radio Frequency Integrated Circuits Symposium (RFIC)*, May 2016, pp. 31–34.

[8] *The Zero Bias Schottky Diode Detector at Temperature Extremes - Problems and Solutions*, Keysight, 11 1999.

[9] U. Tietze, C. Schenk, and E. Gamm, *Electronic Circuits: Handbook for Design and Application*. Springer, 2008, vol. 2.

[10] A. Singh, X. Gao, E. Yavari, M. Zakrzewski, X. H. Cao, V. M. Lubecke, and O. Boric-Lubecke, "Data-based quadrature imbalance compensation for a CW doppler radar system," *IEEE Transactions on Microwave Theory and Techniques*, vol. 61, no. 4, pp. 1718–1724, April 2013.